Organic Electronics 14 (2013) 2192–2197

Contents lists available at SciVerse ScienceDirect

Organic Electronics

journal homepage: www.elsevier.com/locate/orgel

Thermal annealing effect on internal electrical polarization in organic solar cells

Chen Zhao [a], Xianfeng Qiao [a], Bingbing Chen [a], Bin Hu [a,b,*]

[a] WuHan National Laboratory for Optoelectronics and School of Optical and Electronic Information, Huazhong University of Science and Technology, Wu Han 430074, China

[b] Department of Materials Science and Engineering, University of Tennessee, Knoxville, TN 37996, United States

ARTICLE INFO

Article history:
Available online 31 May 2013

Keywords:
Organic solar cells
Electrical polarization
Photocurrent
Donor:acceptor interfaces
Charge transport

ABSTRACT

This article reports experimental studies on internal electrical polarization effects by using optical absorption and photoexcitation assisted capacitance–voltage (*C–V*) measurements based on morphological development in the standard P3HT:PCBM solar cell. We observe that morphological development can increase absorption intensity upon thermal annealing. The increase of absorption intensity essentially reflects an enhancement of absorption coefficient of local donor and acceptor structures. We attribute the enhancement of absorption coefficient to the well-known morphological developments: increased polymer crystallinity and molecular aggregations caused by thermal annealing. Furthermore, the enhancement in absorption coefficient indicates stronger electrical polarizations in the P3HT:PCBM film. The *C–V* studies find that increasing local electrical polarizations can lead to an enhancement on the generation of charge carriers at donor:acceptor interfaces and the transport of generated charge carriers to respective electrode interfaces in the P3HT:PCBM device. Our experimental findings suggest that local electrical polarizations play an important role in the development of photovoltaic processes in organic solar cells.

1. Introduction

Organic bulk-heterojunction solar cells have become an attractive component in photovoltaic devices based on facile tuning of materials parameters, possible fabrication of using printing technique, and mechanically flexible properties [1–6]. Essentially, the morphological development of donor and acceptor interpenetrating networks is a critical issue in controlling internal photovoltaic processes [7–12]. It is noted that the morphological development of donor and acceptor structures is intimately coupled with local electrical polarizations when the donor and acceptor are in excited states [13–15]. Specifically, the local electrical polarizations of donor and acceptor structures can be inevitably changed due to the Coulomb interactions at the interfaces of excited donor:acceptor when donor and acceptor structures are developed into interpenetrating networks. It is further noted that the change of local electrical polarizations can affect light absorption, charge dissociation, and charge transport at donor:acceptor interfaces in the development of photovoltaic functions [16–20]. In this work, we study electrical polarization effects upon morphological development through thermal annealing based on ITO/PEDOT/P3HT:PCBM/Al device by using optical absorption and photoexcitation assisted capacitance–voltage (*C–V*) measurements. Our intention is to elucidate the effects of local electrical polarizations on internal photovoltaic processes in organic bulk-heterojunction solar cells.

2. Experimental section

We use poly(3-hexylthiophene) (P3HT) (purchased from Nanostructured Carbon) as electron donor and

* Corresponding author at: Department of Materials Science and Engineering, University of Tennessee, Knoxville, TN 37996, United States.
E-mail address: bhu@utk.edu (B. Hu).

1566-1199/$ - see front matter © 2013 Elsevier B.V. All rights reserved.
http://dx.doi.org/10.1016/j.orgel.2013.05.016

1-(3-methyloxycarbonyl)propyl-1-phenyl [6,6] C61 (PCBM) (purchased from Luminescence Technology) as the acceptor to fabricate organic bulk-heterojunction solar cells with device architecture of ITO/PEDOT/P3HT:PCBM/Al. The P3HT:PCBM weight ratio was prepared to be 1:0.8 in ortho-dichlorobenzene (ODCB) solution. The photovoltaic films were spin cast with the thickness of 150 nm on precleaned indium tin oxide (ITO) substrates coated with 40 nm thin layer of poly(3,4-ethylenedioxythiophene):poly(styrenesulfonate) (PEDOT:PSS) (Baytron P AI4083). Then 100 nm thick aluminum (Al) electrode was deposited onto the photovoltaic film under the vacuum of 2×10^{-6} Torr. The finished devices are annealed at 150 °C for 10 min in nitrogen gas. For obtaining the absorption spectra, the P3HT:PCBM photovoltaic films were spin cast on the quartz substrates, and a UV-3600 UV–VIS–NIR spectrophotometer was used to measure optical absorption. The photocurrent–voltage characteristics were recorded by using Keithley 2400 source meter under illumination of AM 1.5G 100 mW/cm^2 from Newport solar simulator. The photoexcitation assisted *C–V* measurements were performed by using a dielectric spectrometer (Agilent, 4294A) with alternating voltage of 50 mV at 1 kHz. All measurements were performed at room temperature in inert atmosphere.

3. Results and discussion

Fig. 1a shows the optical absorption for the P3HT:PCBM blend film measured before and after annealing. We can see that thermal annealing leads to an increase on absorption intensity in the range from 450 nm to 550 nm. The calculation indicates that the optical absorption intensity is increased by 4.35% upon thermal annealing. Because the P3HT:PCBM film thickness maintains un-changed during the thermal annealing, the increase of absorption intensity indeed reflects an enhancement on absorption coefficient of P3HT:PCBM film. We know that absorption coefficient is defined as the probability that an incident photon can be absorbed by a given molecule. This probability is determined by the interaction between incident photon (electromagnetic field) and induced electrical dipole. A stronger electrical polarization can lead to a larger electrical dipole. The enhancement in absorption coefficient can thus suggest a stronger electrical polarization in the P3HT:PCBM film. Morphological studies have shown that thermal annealing can increase the crystallinity of the P3HT structure and the aggregations of PCBM molecules [21–23]. This can lead to an enhancement on photovoltaic performance in the ITO/PEDOT/P3HT:PCBM/Al device (Fig. 1b). We should note that the polymer crystallinity and molecular aggregations can increase inter-chain and inter-molecular Coulomb interactions in excited states under photoexcitation. Consequently, the Coulomb interaction between P3HT and PCBM structures at the donor:acceptor interfaces can be increased upon morphological development of donor and acceptor interpenetrating networks. In principle, developing donor and acceptor interpenetrating morphologies can inevitably modify the local polarizations, changing photovoltaic functions in organic solar cells.

Fig. 2 schematically shows the development of electrical polarizations in bulk photovoltaic film and electrode interfaces in dark and under photoexcitation conditions. Due to work function difference, ITO (hole collecting electrode) and Al (electron collecting electrode) become negative and positive surfaces, respectively, caused by the charge tunneling through photovoltaic film between two electrodes under dark condition (Fig. 2a). The negative ITO and positive Al surface carry charge carriers: $-Q_e$ and $+Q_e$, respectively. More importantly, the difference in work function between anode and cathode generates a built-in electric field across a photovoltaic film in an organic solar cell. Essentially, the local P3HT and PCBM structures become electrically polarized in excited states under the influence of built-in electric field. It is noted that the electrical polarizations in P3HT and PCBM structures do not generate net charge carriers but can dominantly determine the absorption coefficient of photovoltaic P3HT:PCBM film by interacting with an incident electromagnetic wave. Therefore, measurement of absorption coefficient can elucidate internal electrical polarization in an organic solar cell. On the other hand, the electrical polarization can lead to net charges, namely surface charges (Q_s) on the surfaces of a photovoltaic film under dark condition (Fig. 2b). Obviously, changing local electrical polarizations can modify the density of surface charges. Clearly, the surface charges Q_s and electrode charges Q_e have opposite signs. The effective charges Q_{eff} at organic/electrode interfaces can be given by:

$$Q_{\text{eff}} = Q_e - Q_s \tag{1}$$

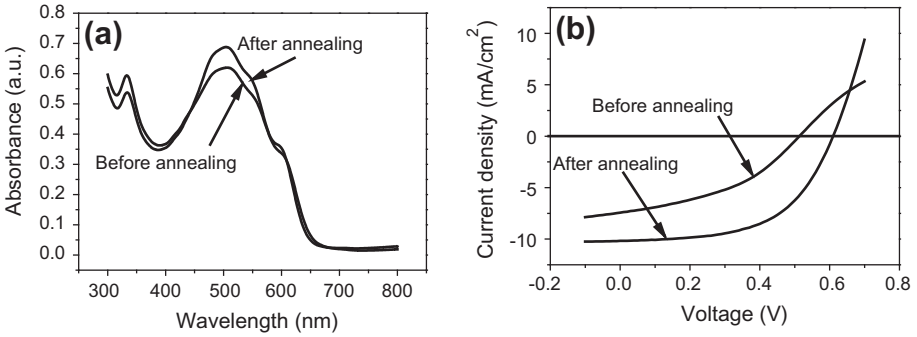

Fig. 1. (a) UV–VIS absorption spectra of P3HT:PCBM film before and after annealing. (b) Current–voltage (*I–V*) characteristics. The measurements were performed on ITO/PEDOT/P3HT:PCBM/Al device before and after annealing.

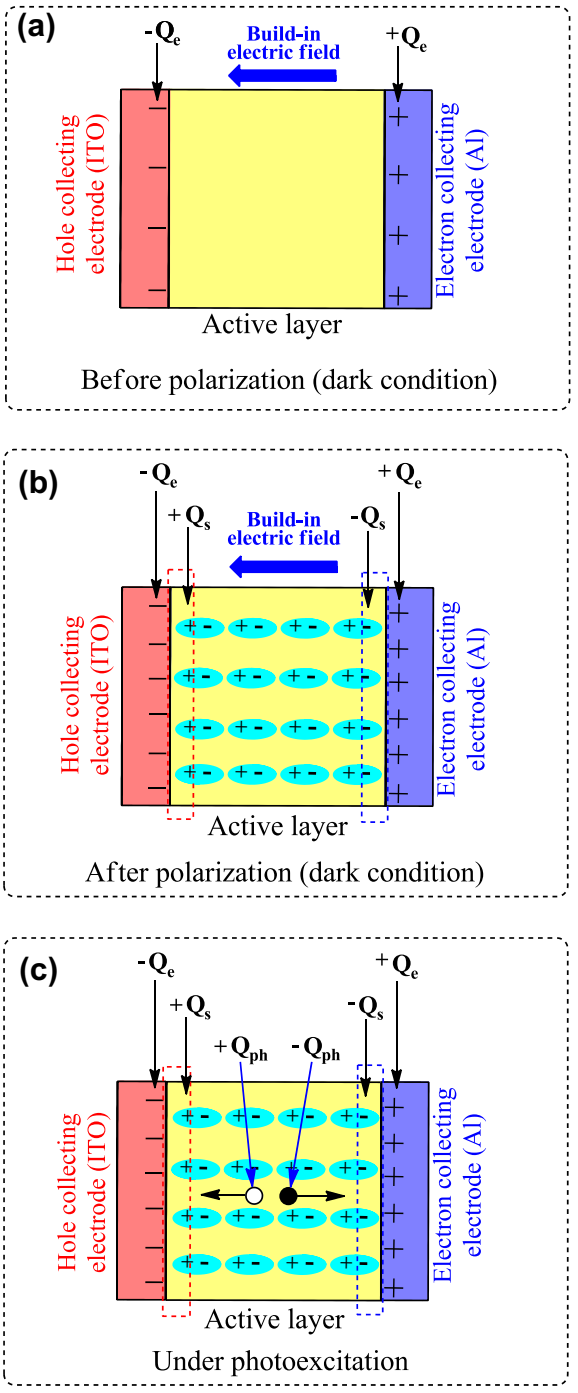

Fig. 2. Development of electrical polarization in an organic solar cell. (a) Situation before polarization occurs. $-Q_e$ and $+Q_e$ represent the electrode charges generated by the workfunction difference in dark condition. (b) Situation with electrical polarization. The surface charges Q_s are generated by electrical polarization and appear on the surface of the photovoltaic film. In dark condition, the charges at organic/electrode interfaces include both surface charges Q_s and electrode charges Q_e. (c) Situation under photoexcitation. The photo-generated carriers $+Q_{ph}$ (open circle) and $-Q_{ph}$ (filled circle) are collected by ITO and Al electrodes. In this case, the organic/electrode interfaces contain electrode charges Q_e in dark, surface charges Q_s in dark, and photo-generated charges Q_{ph} under photoexcitation.

where the surface charges Q_s is a function of local polarization, the electrode charges Q_e is a function of charge tunneling. We further note that the effective charges Q_{eff} can be determined by C–V measurement in a simple capacitance model, as shown in the following equation.

$$CV = Q_{eff} = Q_e - Q_s \quad (2)$$

Under photoexcitation, the photo-generated carriers $+Q_{ph}$ and $-Q_{ph}$ will be collected by ITO and Al electrode under the influence of built-in electric field (Fig. 2c). Therefore, the effective charges (Q^*_{eff}) under photoexcitation contain three components: electrode charges (Q_e) under dark, surface charges (Q_s) under dark, and photo-generated charges (Q_{ph}), given by:

$$CV = Q^*_{eff} = Q_e - Q_s - Q_{ph} \quad (3)$$

Therefore, measuring capacitance in dark condition and under photoexcitation can reflect the interfacial polarization when donor and acceptor morphological structures are changed through thermal or solvent annealing.

Now, we use C–V measurements in dark condition to analyze the electrical polarization in the ITO/PEDOT/P3HT:PCBM/Al device when morphological structures are developed by thermal annealing. Fig. 3 shows the C–V characteristics measured before and after thermal annealing under dark condition. The C–V characteristics indicate following three points. First, at zero bias, the ITO/PEDOT/P3HT:PCBM/Al device shows smaller and larger effective capacitance: 2.14 nF and 2.54 nF under the conditions before and after thermal annealing, respectively. This C–V result confirms that thermal annealing increases the electrical polarization of P3HT:PCBM film in the ITO/PEDOT/P3HT:PCBM/Al device. Second, the effective capacitance quickly increases as applied bias changes from 0 V to V_{peak}. The increase in effective capacitance comes from the fact that changing bias towards the V_{peak} leads to a decrease on the effective electric field (E_{eff}) combining applied field (E_{app}) and built-in field components (E_{bt}) (Eq. (4)).

$$E_{eff} = E_{bt} - E_{app} \quad (4)$$

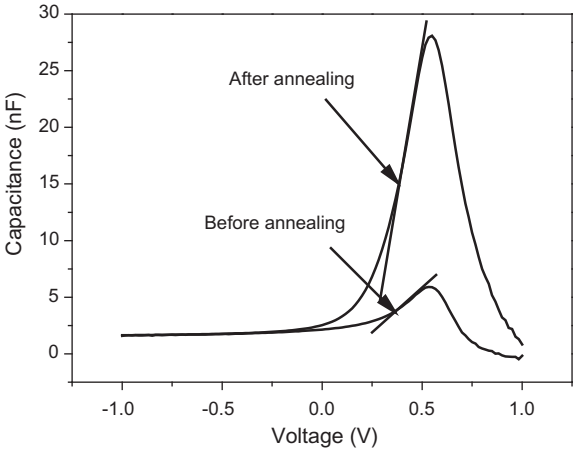

Fig. 3. Capacitance–voltage (C–V) characteristics under dark condition for ITO/PEDOT/P3HT:PCBM/Al device measured before and after annealing.

Decreasing the effective field can reduce the electrical polarization and consequently the surface charges, leading to an increase on the effective charges Q_{eff} ($Q_{eff} = Q_e - Q_s$, we should note that during the *I–V* measurement the electrode charges Q_e do not change before charge injection at V_{OC}). This can be reflected as a quick increase on the capacitance in the *C–V* measurements in dark condition as the applied bias approaches to V_{peak}. More importantly, the increasing rate of capacitance-to-voltage after annealing is much larger than that before annealing (Fig. 3). The capacitance increasing rate $\left(\frac{\Delta C}{V}\right)$ can be determined by the slope of *C–V* curve to be 89.2 nF/V after annealing and 14.5 nF/V before annealing, by a factor of 6.2. This experimental result implies that the electrical polarizability $\left(\frac{\Delta\varepsilon}{E}\right)$ of photovoltaic P3HT:PCBM film, defined as the change in dielectric constant ($\Delta\varepsilon$) to applied electric field (E), becomes much larger after annealing than before annealing. We should note that a larger electrical polarizability $\left(\frac{\Delta\varepsilon}{E}\right)$ corresponds to a lower binding energy of an electron–hole pair upon incident electromagnetic waves of photoexcitation. Third, when the applied bias increases beyond the V_{peak}, the capacitance quickly decreases under dark condition. This means that the amount of effective charges (Q_{eff}) begins decreasing at the V_{peak}. We know that at the V_{peak} the applied bias induces charge injection from respective electrodes into the photovoltaic P3HT:PCBM film. It should be pointed out that the injected charges have opposite signs relative to effective charge carriers at each surface of photovoltaic P3HT:PCBM film. Therefore, injecting charge carriers into the P3HT:PCBM film can decrease the amount of effective charge carriers (Q_{eff}), leading to a reduction on the capacitance in the ITO/PEDOT/P3HT:PCBM/Al device when the applied bias is greater than V_{peak}. We can see from Fig. 3 that the *C–V* measurements before and after annealing give smaller and larger capacitance decreasing rates at the applied bias greater than V_{peak}. The larger capacitance decreasing rate of annealed P3HT:PCBM device when applied bias continues to increase after V_{peak} also suggests that thermal annealing increases the electrical polarizability of P3HT:PCBM film. In addition, we can see in Fig. 3 that the thermal annealing causes a slight increase on V_{peak} changing from 0.533 V to 0.550 V. It is noted that the V_{peak}, where the charge injection begins in dark condition, is determined by the potential barrier at organic/electrode interface. The experimental studies have found that the potential barrier at organic/electrode interface can be changed by surface defects of photovoltaic film [24–28]. Especially, thermal annealing can lead to a decrease on the density of structural defects [29–31]. Here, the observed V_{peak} shift can directly confirm that thermal annealing can reduce the density of surface defects of P3HT:PCBM film.

Now we discuss the *C–V* characteristics under photoexcitation measured before and after annealing. Similarly to the dark *C–V* characteristics shown in Fig. 3, we can see from Fig. 4 that the capacitance shows three interesting changes upon thermal annealing under photoexcitation. First, at zero bias, the capacitance difference between annealing and unannealing conditions under photoexcitation is much larger than that under dark condition. We should note that the capacitance under photoexcitation

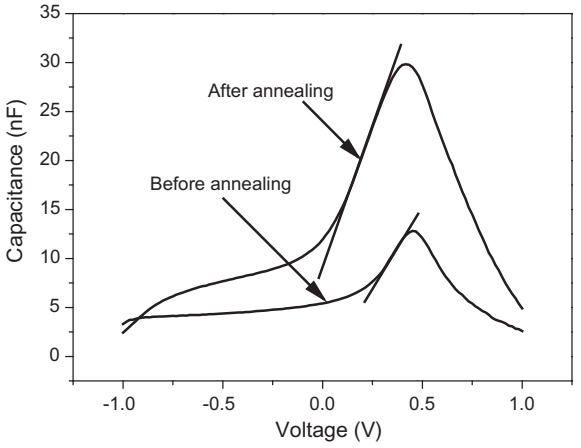

Fig. 4. Capacitance–voltage (*C–V*) characteristics under photoexcitation condition for ITO/PEDOT/P3HT:PCBM/Al device measured before and after annealing.

contains large amount of photo-generated charges in an organic solar cell. Therefore, the capacitance difference at zero bias under photoexcitation reflects the generation of photo-generated charges before and after thermal annealing. We can thus suggest that the increased electrical polarization induced by thermal annealing can contribute to the generation of photo-generated charges through exciton dissociation. Second, the capacitance quickly increase as applied bias changes from 0 V to V_{peak}. This means that the photo-generated charge carriers largely accumulate due to traps at electrode interfaces as the applied bias increases to V_{peak} in both un-annealed and annealed devices. In particular, the capacitance increasing rate becomes larger after annealing than that before annealing under photoexcitation when the applied bias increases to V_{peak}. The capacitance increasing rates are determined to be 55.4 nF/V after annealing and 31.1 nF/V before annealing. This means that the effective charges (Q^*_{eff}) under photoexcitation detected at electrode interfaces increases much faster after annealing than that before annealing. As indicated in Eq. (3), the Q^*_{eff} under photoexcitation includes Q_e (electrode charges) and Q_s (surface charges) under dark, and Q_{ph} (photo-generated charges). Assuming that the photo-generated charges (Q_{ph}) is a dominant component in the effective charge carriers (Q^*_{eff}) under photoexcitation, the effective charges (Q^*_{eff}) can approximately be similar to photo-generated charges (Q_{ph}) as shown in the following equation:

$$Q^*_{eff} \approx -Q_{ph} \tag{5}$$

The photo-generated charges can then be determined by the capacitance measured under photoexcitation condition [32–34].

$$C^{-2} = \frac{2V_{eff}}{\varepsilon_0 \varepsilon Q_{ph}} \tag{6}$$

where the V_{eff} is effective potential, ε_0 and ε are vaccum permittivity and dielectric constant, respectively. Both ε_0 and ε are involved in geometrical value:

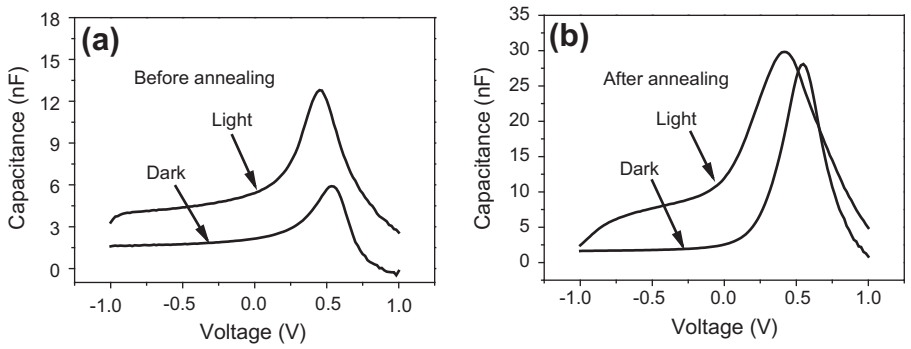

Fig. 5. (a) Comparison of capacitance–voltage (C–V) characteristics between photoexcitation and dark conditions. (a) C–V before annealing. (b) C–V after annealing. Replotted from the data of Figs. 3 and 4.

$$C_g = \frac{A\varepsilon_0\varepsilon}{L} \tag{7}$$

where the A is the area of device, and L is for the active layer thickness. By combining Eqs. (6) and (7), we can calculate the increasing rates $\left(\frac{\Delta Q_{photo}}{V}\right)$ of photo-generated charges to applied bias to be 49.95 nF and 5.49 nF for annealing and unannealing conditions under photoexcitation when the applied bias increases to V_{peak}, by a factor of 9.1. We know that the increasing rate of photo-generated charges to applied field reflects the charge transport. A larger increasing rate of photo-generated charges to applied field corresponds to a stronger transport of photo-generated charges when local electrical polarizations are increased by morphological development through thermal annealing. It is noted from literature results that thermal annealing can largely enhance the transport channels through morphological development in bulk-heterojunction solar cells [10,21,35,36]. Here, our C–V studies under photoexcitation find that the increased electrical polarization upon morphological development plays an important role in the transport of photo-generated charges in the generation of photocurrent. Third, the capacitance quickly decreases as the applied bias increases beyond the V_{peak}, due to the charge recombination and charge injection. We see photoexcitation leads to a larger V_{peak} shift (0.450 V − 0.417 V = 0.033 V) between annealing and unannealing conditions as compared to that (0.550 V − 0.533 V = 0.017 V) under dark condition. Because the charge accumulation causes the V_{peak} shift, the larger V_{peak} shift indicates that photo-generated charges are more accumulated on the surfaces of photovoltaic film after annealing, ready to be involved in the charge injection at V_{peak}. Therefore, characterizing V_{peak} can reveal the accumulation of photo-generated charges at organic/electrode interfaces. We further compare the V_{peak} between dark (Fig. 3) and photoexcitation (Fig. 4) conditions before and after annealing to elucidate the accumulation of photo-generated charges at organic/electrode interfaces (Fig. 5). After annealing, the photoexcitation generates a V_{peak} shift of 0.133 V relative to the dark V_{peak} value. Before annealing, the photoexcitation corresponds to a V_{peak} shift of 0.083 V relative to the dark V_{peak} value. Here, larger/smaller V_{peak} shift means more/less accumulation of photo-generated charges at organic/electrode interfaces. Therefore, the comparison of photoexcitation-induced V_{peak} shift between annealing and dark conditions clearly indicates that the enhanced charge transport by electrical polarizations in annealed device causes an increase on accumulation of photo-generated charges at organic/electrode interfaces.

4. Conclusions

In summary, the internal electrical polarizations are studied by using C–V measurements under dark and photoexcitation conditions upon morphological development through thermal annealing in the standard ITO/PEDOT/P3HT:PCBM/Al device. We demonstrate that morphological development upon thermal annealing can increase the local electrical polarizations of photovoltaic P3HT:PCBM film, which can enhance the optical absorption coefficient, charge generation, and charge transport in the ITO/PEDOT/P3HT:PCBM/Al device. In addition, our C–V results indicate that enhanced charge transport causes an accumulation of photo-generated charge carriers at organic/electrode interfaces due to interfacial traps. Clearly, removing charge accumulation can lead to possibilities of further improving photocurrent. As a result, adjusting electrical polarizations becomes an important method to improve photovoltaic performance in organic bulk-heterojunction solar cells.

Acknowledgements

This research was supported by International Cooperation and Exchange Program (Grant No. 21161160445) and photovoltaic Project (Grant Nos. 61077020 and 61205034) funded by the National Natural Science Foundation of China. The authors also acknowledge the support from National Significant Program (Quantum Control: 2013CB922104). The author (B.H.) acknowledges the financial support from the National Science Foundation (ECCS-1102011) of USA.

References

[1] C.J. Brabec, N.S. Sariciftci, J.C. Hummelen, Adv. Funct. Mater. 11 (2001) 15–26.
[2] K.M. Coakley, M.D. McGehee, Chem. Mater. 16 (2004) 4533–4542.
[3] C.J. Brabec, Sol. Energy Mater. Sol. Cells 83 (2004) 273–292.
[4] J.Y. Kim, K. Lee, N.E. Coates, D. Moses, T.-Q. Nguyen, M. Dante, A.J. Heeger, Science 317 (2007) 222–225.
[5] S. Gunes, H. Neugebauer, N.S. Sariciftci, Chem. Rev. 107 (2007) 1324–1338.
[6] G. Li, R. Zhu, Y. Yang, Nat. Photonics 6 (2012) 153–161.

[7] G. Yu, J. Gao, J.C. Hummelen, F. Wudl, A.J. Heeger, Science 270 (1995) 1789–1791.
[8] M. Granstrom, K. Petritsch, A.C. Arias, A. Lux, M.R. Andersson, R.H. Friend, Nature 395 (1998) 257–260.
[9] F. Padinger, R.S. Rittberger, N.S. Sariciftci, Adv. Funct. Mater. 13 (2003) 85–88.
[10] W. Ma, C. Yang, X. Gong, K. Lee, A.J. Heeger, Adv. Funct. Mater. 15 (2005) 1617–1622.
[11] F. Zhang, K.G. Jespersen, C. Bjorstrom, M. Svensson, M.R. Andersson, V. Sundstrom, K. Magnusson, E. Moons, A. Yartsev, O. Inganas, Adv. Funct. Mater. 16 (2006) 667–674.
[12] L.-M. Chen, Z. Hong, G. Li, Y. Yang, Adv. Mater. 21 (2009) 1434–1449.
[13] T.M. Clarke, A.M. Ballantyne, J. Nelson, D.D.C. Bradley, J.R. Durrant, Adv. Funct. Mater. 18 (2008) 4029–4035.
[14] H. Zang, Z. Xu, B. Hu, J. Phys. Chem. B 114 (2010) 5704–5709.
[15] M. Iwamoto, T. Manaka, Anal. Chim. Acta 568 (2006) 65–69.
[16] M.A. Sefunc, A.K. Okyay, H.V. Demir, Opt. Express 19 (2011) 14200–14209.
[17] V. Coropceanu, J. Cornil, D.A. da Silva Filho, Y. Olivier, R. Silbey, J.-L. Bredas, Chem. Rev. 107 (2007) 926–952.
[18] W.J. Grzegorczyk, T.J. Savenije, M. Heeney, S. Tierney, I. McCulloch, S. van Bavel, L.D.A. Siebbeles, J. Phys. Chem. C 112 (2008) 15973–15979.
[19] K. Vandewal, K. Tvingstedt, A. Gadisa, O. Inganas, J.V. Manca, Nat. Mater. 8 (2009) 904–909.
[20] H. Zang, Y. Liang, L. Yu, B. Hu, Adv. Energy Mater. 1 (2011) 923–929.
[21] X. Yang, J. Loos, S.C. Veenstra, W.J.H. Verhees, M.M. Wienk, J.M. Kroon, M.A.J. Michels, R.A.J. Janssen, Nano Lett. 5 (2005) 579–583.
[22] J. Jo, S.-S. Kim, S.-I. Na, B.-K. Yu, D.-Y. Kim, Adv. Funct. Mater. 19 (2009) 866–874.
[23] T. Erb, U. Zhokhavets, G. Gobsch, S. Raleva, B. Stuhn, P. Schilinsky, C. Waldauf, C.J. Brabec, Adv. Funct. Mater. 15 (2005) 1193–1196.
[24] Y. Park, V.-E. Choong, B.R. Hsieh, C.W. Tang, Y. Gao, Phys. Rev. Lett. 78 (1997) 3955–3958.
[25] H. Ishii, K. Sugiyama, E. Ito, K. Seki, Adv. Mater. 11 (1999) 605–625.
[26] S. Braun, W.R. Salaneck, M. Fahlman, Adv. Mater. 21 (2009) 1450–1472.
[27] T. Sueyoshi, H. Fukagawa, M. Ono, S. Kera, N. Ueno, Appl. Phys. Lett. 95 (2009) 183303.
[28] J.Q. Zhong, H.Y. Mao, R. Wang, D.C. Qi, L. Cao, Y.Z. Wang, W. Chen, J. Phys. Chem. C 115 (2011) 23922–23928.
[29] G.W. Neudeck, T.C. Lee, Appl. Phys. Lett. 43 (1983) 680–682.
[30] T. Sueyoshi, H. Kakuta, M. Ono, K. Sakamoto, S. Kera, N. Ueno, Appl. Phys. Lett. 96 (2010) 093303.
[31] J. Frisch, M. Schubert, E. Preis, J.P. Rabe, D. Neher, U. Scherf, N. Koch, J. Mater. Chem. 22 (2012) 4418–4424.
[32] G. Garcia-Belmonte, A. Munar, E.M. Barea, J. Bisquert, I. Ugarte, R. Pacios, Org. Electron. 9 (2008) 847–851.
[33] P.P. Boix, M.M. Wienk, R.A.J. Janssen, G. Garcia-Belmonte, J. Phys. Chem. C 115 (2011) 15075–15080.
[34] M. Mingebach, C. Deibel, V. Dyakonov, Phys. Rev. B 84 (2011) 153201.
[35] G. Li, V. Shrotriya, J. Huang, Y. Yao, T. Moriarty, K. Emery, Y. Yang, Nat. Mater. 4 (2005) 864–868.
[36] Y. Kim, S. Cook, S.M. Tuladhar, S.A. Choulis, J. Nelson, J.R. Durrant, D.D.C. Bradley, M. Giles, I. Mcculloch, C.-S. Ha, M. Ree, Nat. Mater. 5 (2006) 197–203.